2022 S.T. Yau High School Science Award (Asia)

Research Report

The Team

Registration Number: Phy-149

Name of team member: Juan Zibo
School: National Junior College
Country: Singapore

Name of team member: Feng Siyu
School: National Junior College
Country: Singapore

Name of supervising teacher: Yiren Shen
Job Title: PhD Candidate
School: Stanford University
Country: The United States of America

Title of Research Report

Delaying Tip Stall By Self-adaptive Morphing Wing System

Date

31 August 2021

Delaying Tip Stall By Self-adaptive Morphing Wing System

Juan Zibo, Feng Siyu

31 August 2022

Abstract

Morphing Wing Systems on aircraft provide efficient improvements and optimizations on the aerodynamic performances of wings via continuous changing of their geometric structures. The key advantage of morphing wing systems over traditional wings with ailerons is their ability of changing their airfoil shapes that leads to high adaptability of multiple flight conditions. Previous researchers have developed various ways of morphing, such as dihedral twist, inflatable wings, spanwise trailing edge deflections and so on. While many researchers focused on delaying stall, using morphing wing system to cope with a specific problem, tip stall, has not been investigated.

In this paper, a self-adaptive feedback control morphing wing system by spanwise trailing edge deflections is developed to increase lift and delay tip stall. A morphing configuration of linear deflection from root to tip is introduced. The equations of the deflection curves are derived and the 3D models of morphing wing configurations are built. A series of CFD simulations and actual flight experiments are conducted to study the aerodynamic performances and obtain the aerodynamic database. Optimization is then applied and the self-adaptive

functions are set up with reference to the database. The self-adaptive system contains takeoff-landing function which is able to achieve higher lift and larger stall and cruise-stage function which is able to maintain constant lift coefficient at various angles of attack. By applying the take on NACA-0012 finite wing, stall is delayed from 14° angle of attack to 34° angle of attack and a significant increase in coefficient of lift is also achieved. By applying the cruise-stage function, a high stall angle is achieved which allows the wing to have constant C_L under different AOA through upward deflection.

Keywords: Aerodynamics, Morphing Wing, Tip stall, Self-adaptive system
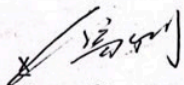
2

Acknowledgement

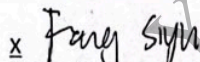**Commitments on Academic Honesty and Integrity**

We hereby declare that we

1. are fully committed to the principle of honesty, integrity and fair play throughout the competition.
2. actually perform the research work ourselves and thus truly understand the content of the work.
3. observe the common standard of academic integrity adopted by most journals and degree theses.
4. have declared all the assistance and contribution we have received from any personnel, agency, institution, etc. for the research work.
5. undertake to avoid getting in touch with assessment panel members in a way that may lead to direct or indirect conflict of interest.
6. undertake to avoid any interaction with assessment panel members that would undermine the neutrality of the panel member and fairness of the assessment process.
7. observe the safety regulations of the laboratory(ies) where the we conduct the experiment(s), if applicable.
8. observe all rules and regulations of the competition.
9. agree that the decision of YHSA(Asia) is final in all matters related to the competition.

We understand and agree that failure to honour the above commitments may lead to disqualification from the competition and/or removal of reward, if applicable; that any unethical deeds, if found, will be disclosed to the school principal of team member(s) and relevant parties if deemed necessary; and that the decision of YHSA(Asia) is final and no appeal will be accepted.

(Signatures of full team below)
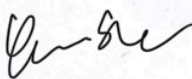
X
Name of team member: Juan Zibo
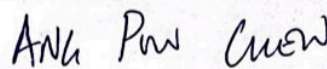
X
Name of team member: Feng Siyu

X
Name of team member:
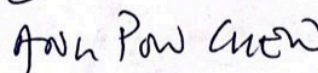
X Yiren SHEN
Name of supervising teacher:

Noted and endorsed by

ANh Pow CHEW
(signature)

Name of school principal: ANh Pow CHEW

4

Contents

1 Introduction

1.1 Background

Morph, a word originated from the Greek word "metamorphosis", means the process of transformation. For aeronautical applications, in the focus on wind design, morphing is most commonly used to denote the techniques that allow the changing of the structure or shape of certain objects. The idea of morphing wing could be originally inspired by the flying bird's features where they constantly change wings geometry while flying. Morphing wing can enhance the aircraft performance, which is the capacity of an aircraft to accomplish certain missions that make it useful to fulfill certain purposes.[1] This enhancement brought by morphing can be realized during various flying phases by twisting its airfoil shapes to adapt the flight conditions with high operating efficiency.
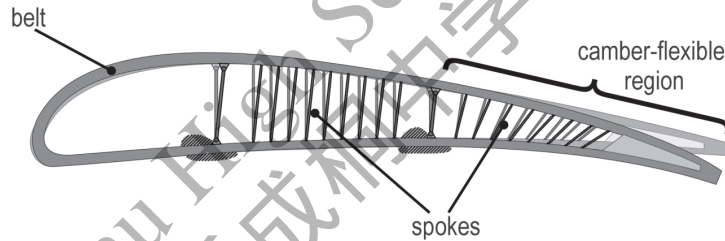
Fig1.1: An example of a morphing wing section

Stall, which is known as a partial or full separation of the airflow over a wing, occurs at a critical angle of attack that a reduction in the lift coefficient is generated. It is where the horizontal line of the wing is at too great of an angle to the apparent wind direction. Thus, the center of pressure on each wing may move in and forward. The aerodynamic center shifts forward relative to center of gravity consequently, leading to the loss of lift, and uncontrollable pitch up of the aircraft if the stabilator fails to counter the pitch up. Tip stall is one type

7

of stalling, in which the wingtip of an airplane before the remainder of the wing is stalled, frequently resulting in the loss of lateral control. As angle of attack increases, the amount of incoming airflow separation also increases thus lift coefficient decreases. During the turning of aircraft, there will be additional apparent wind coming from directly underneath the wing. This will create the effect of bringing the apparent wind direction underneath the wing more than before, increasing the angle of attack and causing the tip of the wing to stall. The tip stalls first in this instance because the tip is moving at faster speed than the root of the wing.
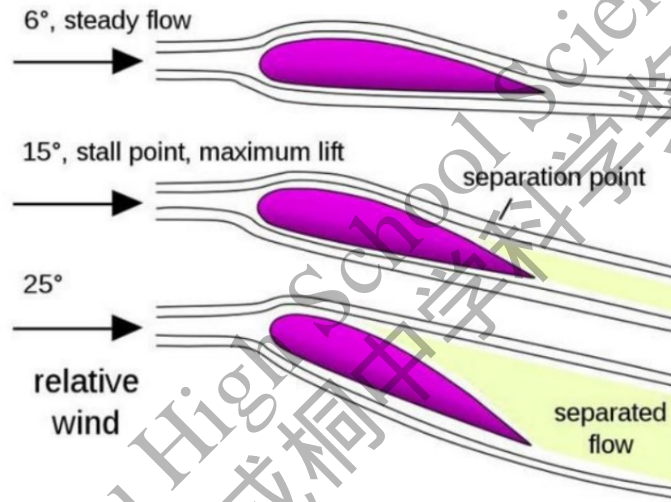
Fig1.2: Demonstration of stall[2]

1.2 Literature Review

The flexible trailing-edge has become the most widely used method for morphing wing designs due to its significant advantages and convenient implementations. The objective of the flexible trailing edge is to achieve a chord-wise and span-wise differential camber variation with the same structural system providing a smooth contour with no additional gaps. The camber variation is centralized at the trailing-edge since this domain has high effectiveness

under both structural and aerodynamic aspects.

Yokozeki.T carried out a wind tunnel experiment to prove that the morphing wing with flexible trailing-edge had better aerodynamic characteristics than a traditional airfoil[3].

Li et al. investigated the aeroelastic response of a morphing flap showing that the critical flutter speed can be reduced by the morphing of airfoil[4]. And a flexible variable camber trailing-edge flap was designed to enhance flight efficiency during takeoff, cruise and landing status[5].

Another application area of the flexible trailing edge is to delay the stall characteristics. Tip stalls have been fatal several times in the history. Some traditional methods to stop tip stalls include the application of vortex generators, stall fence, stall strips and so on. However, as the wing shape affects the formation of stalls, morphing wing system would be a modern solution to deal with the stall characteristics more efficiently. Even though the previous researcher Zi KAN have also investigated the periodic deflection of the flexible trailing-edge with a small deflection amplitude and high deflection rate can delay stall of morphing wing by increasing lift coefficients at the critical stall angle, these existing researches did not specialize the application of morphing wing using for delay tip stall specifically[6]. Therefore, this study serves to design a self-adaptive feedback control morphing wing system to effectively delay tip stall effects by the trailing-edge deflection.

1.3 Section Overview

This work aims to develop a self-adaptive feedback control morphing wing system by multiple spanwise trailing edge deflections. Our work contains three stages. Firstly, the equation of deflection curves are derived by polynomial regression and the 3D models are built with SolidWorks. A 3D simulation of the morphing segment based on fluid dynamics equations of inviscid compressible flow using computational fluid dynamics (CFD) software is conducted.

We have tested the aerodynamic performances of a finite NACA 0012 wing segment under various deflection angles and angles of attack. This stage provides us a database for this specific wing segment and hence determine the efficient morphing scale with regard to different flow conditions respectively. Secondly,the actual morphing wing segment is fabricated and embedded on a radio control(RC) model plane. Actual flight experiments are carried out to verify our simulation work. Lastly, a self-adaptive feedback control system based on the database obtained is introduced. The system is able to detect the current flow condition and adjust automatically to the corresponding optimized morphing shape. With this system, air crafts will be able to delay tip stall and obtain better lateral control in various flow condition.

2   Modeling and Design

In this research, NACA-0012 airfoil with a flexible trailing-edge is adopted for modeling and design. Due to manufacturing technics and material limitation, a wing configuration of 350mm chord length, 1200mm wing span is proposed. The morphing section of the morphing wing is in the 60%-100% chord of the airfoil, and the fixed section is in the 0-60% chord of the airfoil. Angle between the chord line and the line connecting the initial deflecting point and trailing-edge end point is the deflection angle θ which varies between $\pm 20°$ and are selected with 4° intervals.
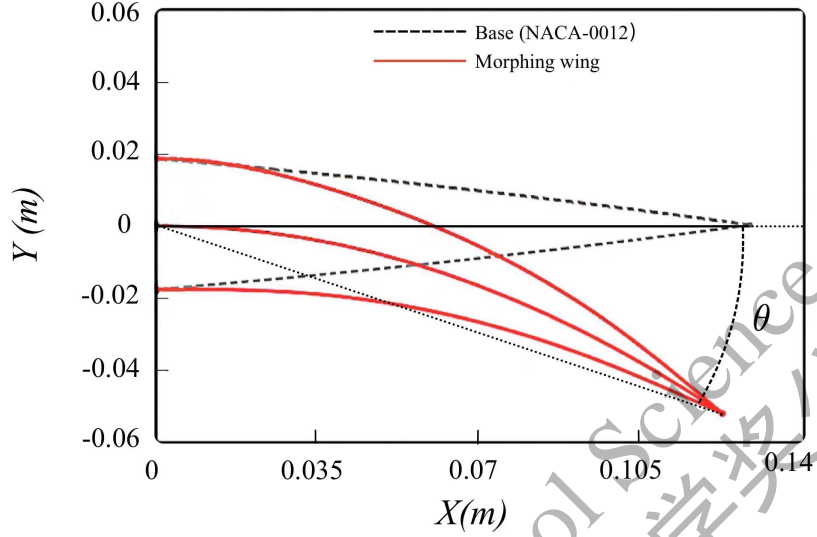
2.1 Modeling Method

Fig2.1: Morphing airfoil

Based on previous researches[6], this study chose to adopt a parabolic camber line of the morphing section. As shown in Fig 2.1, a Cartesian Plane is created and the initial morphing point is set as the origin of coordinates (0, 0). The trajectory equation of camber line can be written as:

$$y = \frac{\tan\theta}{l} \cdot x^2 \tag{1}$$

where l is the length of morphing camber line and is the deflection angle. Since the length of camber line is 140mm which will remain unchanged during the morphing process, by integrating along the camber line:

$$\int_0^\xi \sqrt{1 + 4C^2 x^2}\, \mathrm{d}x, \quad \text{where } C \equiv \frac{\tan\theta}{l}$$

11

the x-coordinate of the morphing trailing edge end point x' can be obtained by the following equation:

$$\frac{\ln\left(\left|\frac{\sqrt{4C^2\xi^2+1}+2C\xi}{4C}\right|\right)}{4C} + \frac{\xi\sqrt{4C^2\xi^2+1}}{2} = 14 \tag{2}$$

Hence the coordinates of the morphing trailing edge end point (ξ, η) can be obtained by substituting the value of ξ in to Equation (2.1). The coordinates of points on upper and lower surfaces can be expressed as:

$$\begin{pmatrix} x_i^{up} \\ y_i^{up} \\ x_i^{low} \\ y_i^{low} \end{pmatrix} = \begin{pmatrix} x_i + Z_i \cdot sin(tan^{-1}(2Cx_i)) \\ y_i + Z_i \cdot cos(tan^{-1}(2Cx_i)) \\ x_i - Z_i \cdot sin(tan^{-1}(2Cx_i)) \\ y_i - Z_i \cdot cos(tan^{-1}(2Cx_i)) \end{pmatrix} \tag{3}$$

where (x_i, y_i) are the coordinates of points on camber line and Z_i is the thickness of original NACA-0012 airfoil. Hence the equations of the upper and lower surfaces can be derived by polynomial regression:

$$y = \beta_0 + \beta_1 x + \beta_2 x^2 + \cdots + \beta_m x^m \tag{4}$$

In matrix form:

$$\begin{bmatrix} y_1 \\ y_2 \\ y_3 \\ \vdots \\ y_n \end{bmatrix} = \begin{bmatrix} 1 & x_1 & x_1^2 & \ldots & x_1^m \\ 1 & x_2 & x_2^2 & \ldots & x_2^m \\ 1 & x_3 & x_3^2 & \ldots & x_3^m \\ \vdots & \vdots & \vdots & \ddots & \vdots \\ 1 & x_n & x_n^2 & \ldots & x_n^m \end{bmatrix} \begin{bmatrix} \beta_0 \\ \beta_1 \\ \beta_2 \\ \vdots \\ \beta_m \end{bmatrix}$$

(5)

which when using pure matrix notation is written as:

$$\vec{y} = \mathbf{X}\vec{\beta} \tag{6}$$

Using ordinary least squares estimation, the vector of estimated polynomial regression coefficients is:

$$\vec{\beta} = (\mathbf{X}^T\mathbf{X})^{-1}\mathbf{X}^T\vec{y} \tag{7}$$

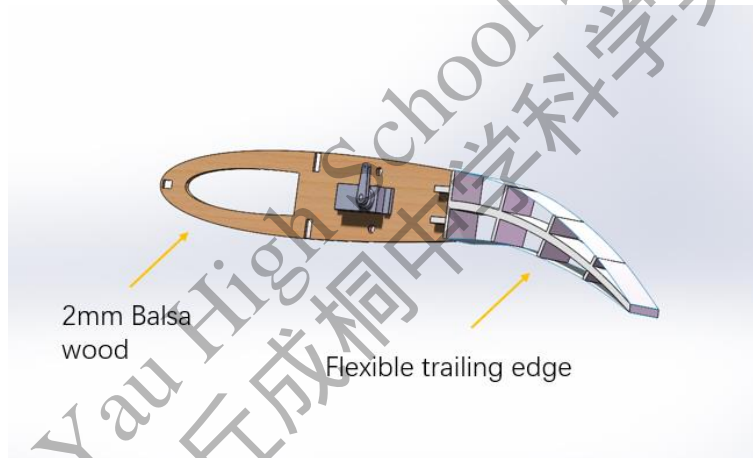## 2.2 Structural Design

2.2.1 Design of Morphing Section

Fig2.2: Design of morphing section

In order to achieve efficient flow control and ensure the structural stability of the wing, a fixed section of 210mm length at 0% to 60% and a morphing section of 140mm length at the 60% to 100% are adopted on each wing rib. The fixed section should be made of wood and the morphing section should be made of flexible material that can easily be bent. The width of the morphing section is around 35mm, and the thickness of the beam is 20mm while the thickness of the other structures are 10mm. A 9g servo is installed at 45% chord of the airfoil

13

to generate sufficient torque for the deflecting trailing edge to bend. An iron wire is attached to the servo and the trailing edge end point. The pulling of the wire by servo will lead to upward deflection of the morphing trailing edge, and the pushing of the wire by servo will lead to downward deflection.

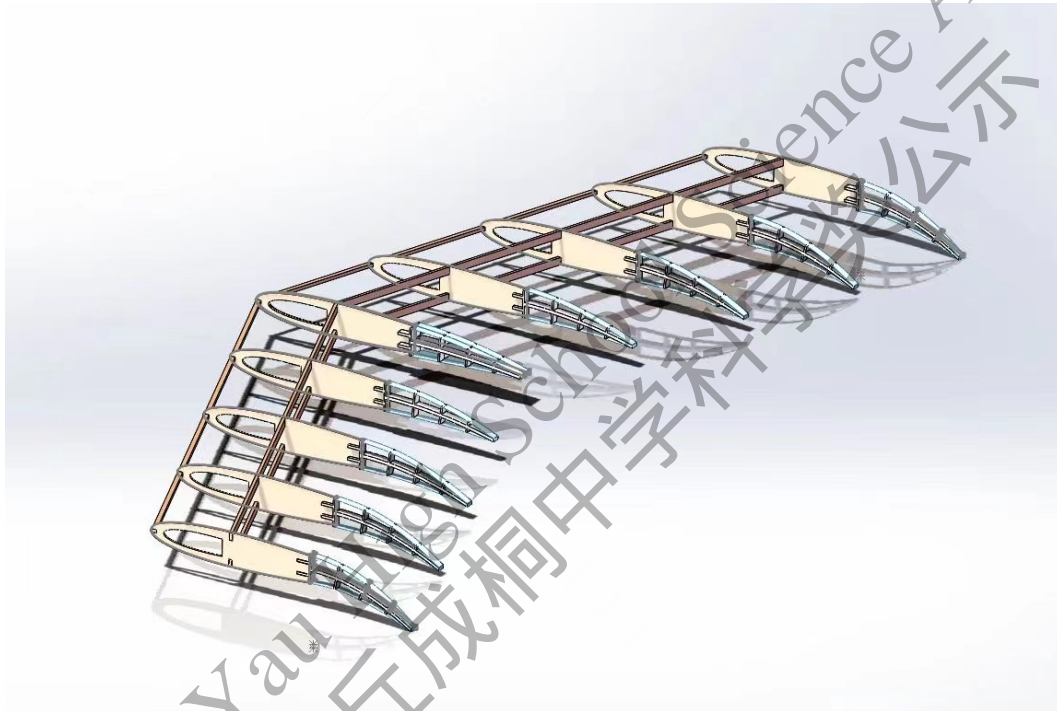### 2.2.2 Design of the morphing wing

Fig2.3: Structure of the wing

The 3D model of the complete wing is assembled in SOLIDWORKS. Each side of the wing contains 4 morphing sections which are able to achieve morphing angle of $\pm 20°$. This is to achieve linear morphing from $0°$ at root to intended morphing angle at tips. The models of configurations which can be used for simulation are obtained by covering all the surfaces of the wing structure. Below shows the model of $20°$ downward morphing configuration as an example.
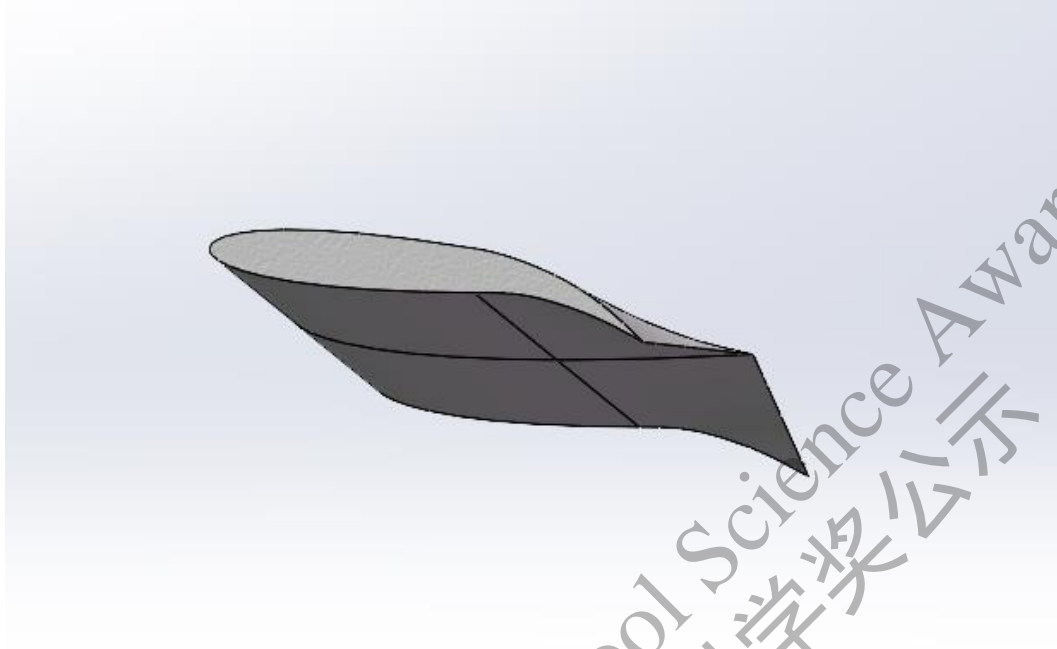
14

Fig2.4: Model of 20° downward morphing configuration

3   CFD Simulation

We chose to use SU2 to conduct Computational Fluid Dynamics(CFD) simulation for this research and the complete process of CFD simulation is exhibited by the flowchart:
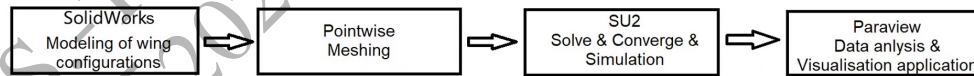

Fig3.1: Flowchart of simulation process

3D models built in SOLIDWORKS are exported into Pointwise, an open source meshing software for meshing. Meshes of different configurations are then loaded in to SU2 for CFD

simulation. Output result of SU2 are exported into Paraview for post-poccess and fluid domain observation.

3.1 Simulation Methodologies

3.1.1 Theory and Governing Equations of SU2

Compressible Euler Equations[7]

Differential form of compressible Navier-Stokes equations can be expressed as:

$$\mathcal{R}(U) = \frac{\partial U}{\partial t} + \nabla \cdot \bar{F}^c(U) - \nabla \cdot \bar{F}^c(U, \nabla U) - S = 0 \tag{8}$$

where the conservative variables are the working variables and given by:

$$U = \{\rho, \rho\bar{v}, \rho E\}^T \tag{9}$$

Compressible Euler equations are obtained as a simplification of the compressible Navier-Stokes equations in the absence of viscosity and thermal conductivity. They can be expressed in differential form as:

$$\mathcal{R}(U) = \frac{\partial U}{\partial t} + \nabla \cdot \bar{F}^c(U) - S = 0 \tag{10}$$

S is a generic source term, and the convective fluxes are:

$$\bar{F}^c = \left\{ \begin{array}{c} \rho\bar{v} \\ \rho\bar{v} \oplus \bar{v} + \bar{\bar{I}}p \\ \rho E\bar{v} + p\bar{v} \end{array} \right\} \tag{11}$$

where ρ is the fluid density, $\bar{v} = \{u, v, w,\}^T \in \mathbb{R}^3$ is the flow speed in Cartesian system of reference, E is the total energy per unit mass, p is the static pressure, $\bar{\bar{\tau}}$ is the viscous stress tensor, T is the temperature.Assuming a perfect gas with a ratio of specific heats γ and gas constant R,one can close the system by determining pressure from $p = (\gamma - 1)\rho[E - 0.5(\bar{v} \cdot \bar{v})]$

16

and temperature from the ideal gas equation of state $T = p/(\rho R)$.

Dimensionless Coefficients

The dimensionless force and moment coefficients are defined as follows[8]. Let ρ_∞ and V_∞ be the pressure and velocity, respectively, in the freestream, far ahead of the body. The freestream dynamic pressure is defined as:

$$q_\infty \equiv \frac{1}{2}\rho_\infty V_\infty^2 \tag{12}$$

The dynamic pressure has the units of pressure. In addition, let S be a reference area and l be a reference length. The dimensionless force and moment coefficients are defined as follows:

Lift coefficient:	$C_L \equiv \dfrac{L}{q_\infty S}$
Drag coefficient:	$C_D \equiv \dfrac{D}{q_\infty S}$
Normal force coefficient:	$C_N \equiv \dfrac{N}{q_\infty S}$
Axial force coefficient:	$C_A \equiv \dfrac{A}{q_\infty S}$
Moment coefficient:	$C_M \equiv \dfrac{M}{q_\infty S l}$

Thin Airfoil Theory[8]

Thin airfoil theory for a cambered airfoil is a generalization of the method for a symmetric airfoil. The lift per unit span of a finite wing can be expressed as:

$$L' = \rho_\infty V_\infty^2 c(\pi A_0 + \frac{\pi}{2}A_1) \tag{13}$$

where the coefficients A_0 and A_1 are given by:

$$A_0 = \alpha - \frac{1}{\pi}\int_0^\pi \frac{dz}{dx}d\theta_0 \tag{14}$$

17

and

$$A_n = \frac{2}{\pi} \int_0^\pi \frac{dz}{dx} \cos n\theta_0 d\theta_0 \qquad (15)$$

A_0 depends on both α and the shape of the camber line (through dz/dx), while the values of A_n depend only on the shape of the camber line. Hence the lift coefficient can be expressed as:

$$C_L = \frac{L'}{\frac{1}{2}\rho_\infty V_\infty^2 c(1)} = \pi(2A_0 + a_1) \qquad (16)$$

By substituting Equation18 and Equation 19, Equation20 becomes:

$$C_L = 2\pi \left[\alpha + \frac{1}{\pi} \int_0^\pi \frac{dz}{dx}(\cos\theta_0 - 1)d\theta_0 \right] \qquad (17)$$

and

$$\text{Lift slope} \equiv \frac{dC_L}{d\alpha} = 2\pi$$

Hence it is clear that:

$$C_L = 2\pi(\alpha - \alpha_{L=0}) \qquad (18)$$

where $\alpha_{L=0}$ denotes the angle of zero lift and is a negative value.

3.1.2 Meshing

In order to achieve accurate computation, obtain nice resolution of wake behind the morphing trailing edge and remain a moderate cell number for computational efficiency, a structured C-H mesh topology is generated on the flow domain and surface of finite wing in Pointwise.

3.2 Computational Details

CFD simulations are conducted on different morphing configurations to study and compare their aerodynamic performances.The basic NACA-0012 finite wing is designed to have 1200mm wing span, 350mm chord length and aspect ratio $AR = b/c = 3.429$. The Reynolds
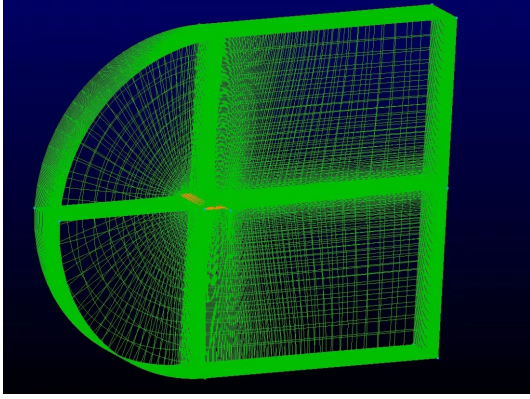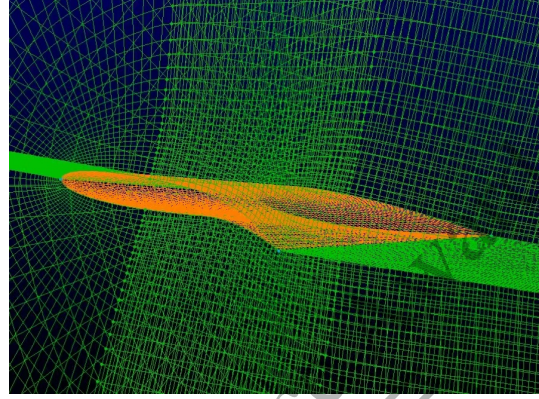
Figure 1: Fig3.3 (a)

Figure 2: Fig3.3 (b)

number based on the wing chord is $Re_c = 2.463 \times 10^5$. In order to simulate general cruise condition of Radio-controlled(RC) aircraft a low Mach number of $M_\infty = 0.0294117647$ is selected as freestream velocity V_∞. The intentioned database of CFD simulation can be expressed as an 11×11 matrix:

$$\mathbf{D} = \begin{bmatrix} S_{11} & S_{12} & S_{13} & \dots & S_{1n} \\ S_{21} & S_{22} & S_{23} & \dots & S_{2n} \\ S_{31} & S_{32} & S_{33} & \dots & S_{3n} \\ \vdots & \vdots & \vdots & \ddots & \vdots \\ S_{n1} & S_{n2} & S_{n3} & \dots & S_{nn} \end{bmatrix} \tag{19}$$

where $n = 11$ and each element in $\mathbf{D}$, S_{ij} is a dataset contains L, D, C_L, C_D and flow field at ith Angle of Attack α and jth deflection angle θ. To obtain detailed database for self-adaptive system, 11 values of α from 10° to 30° are selected with 2° interval; 11 values of θ from -20° to 20° are selected with 4° interval where downward deflection is defined as the positive direction of θ.

19

3.3 Results and Discussion

In this section, the aerodynamic performances of the morphing wing with flexible trailing-edge under different flow conditions and different morphing configurations are studied. The aerodynamic characteristics of different deflection angles are provided and a static database is built for self-adaptive system.
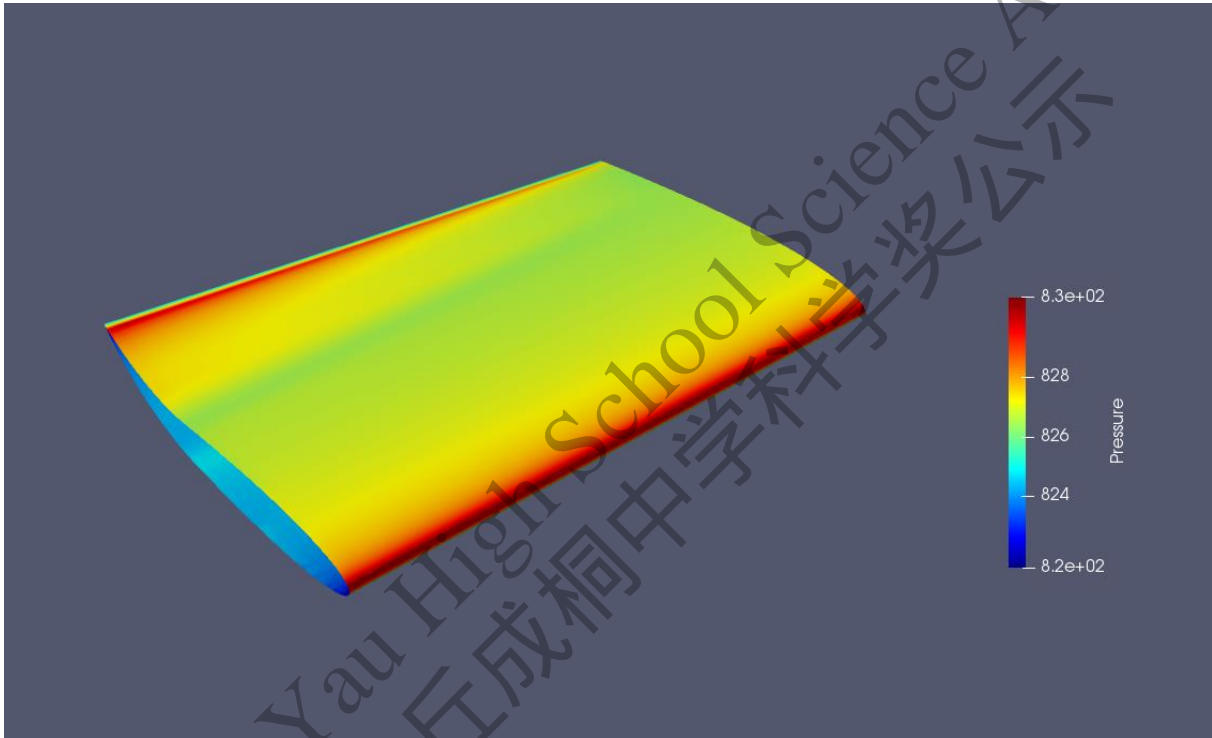

Fig3.4: Pressure distribution on 20° downward deflection at 30° angle of attack

The pressure distribution of 20° downward deflection at 30° angle of attack is presented as an example. The vertical axis is reversed to give a better view of pressure distribution on the lower surface. It can be clearly observed that the pressure on trailing-edge increases along the span from root to tip. This provides extra lift near the tip to delay tip stall.

3.3.1   Effect of trailing-edge deflection on coefficient of lift

The graphs of coefficient of lift C_L and angle of attack α are plotted:
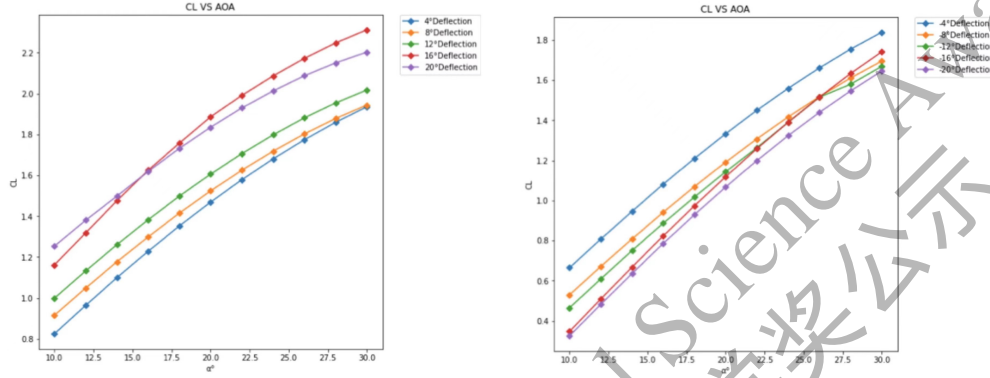

Fig3.5: Coefficient of lift over angle of attack

As shown in Fig3.5, the C_L generally increases with the increase of angle of attack for each deflection angle respectively. 20° downward deflection gives the largest C_L from 10° to 16° angle of attack while 16° downward deflection gives the largest C_L from 16° to 13° angle of attack. The gradient of 4° downward deflection is 0.064 which is close to the $\dfrac{dC_L}{d\alpha}$ of NACA-0012 finite wing calculated by Thin Airfoil Theory, which is 0.05. With the increase in deflection angle, the gradients of curves generally decreases which follows the thin airfoil theory and cambered airfoil theory. Even though the CFD simulation is conducted under compressible flow, this method can still be used to check the validity of data to some extent. Graphs of C_L over morphing angle is also presented to give better illustration:
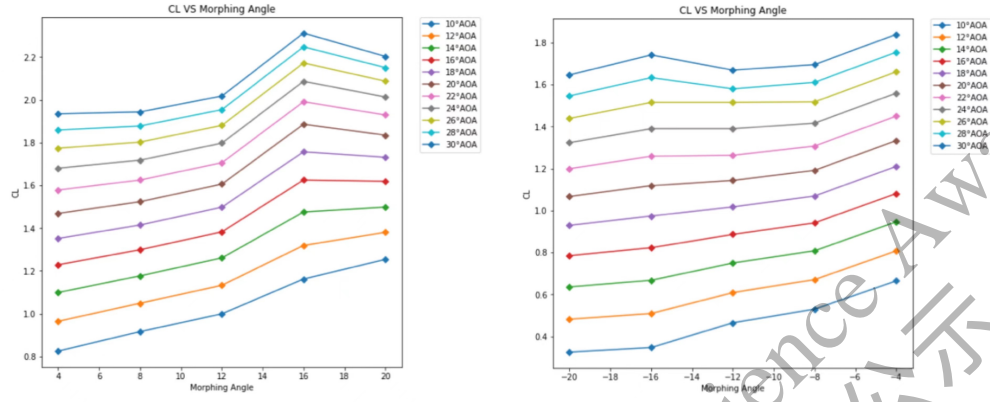
Fig3.6: Coefficient of lift over morphing angle

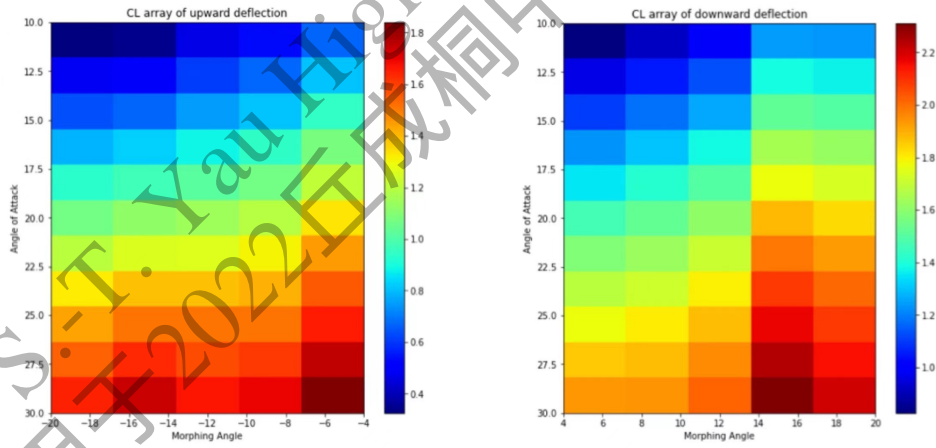The complete database obtained can be shown as the following heat maps:

Fig3.7: Aerodynamic database of C_L

where the x-axis is the deflection angle, y-axis is the angle of attack and the intensity of each

color block represents the C_L at the corresponding condition. By selecting the morphing angle correspond to the appropriate C_L needed at each angle of attack according to this database, the framework of self-adaptive system can be built.

3.3.2 Delaying tip stall

Stall can be better observed by plotting the coefficient of moment along vertical axis CMY over angle of attack. The results indicates that 16°, 20° and $-12°$ deflections lead to significant increase in stall angle. The graph of CMY over α of 20° deflection is shown as an example:
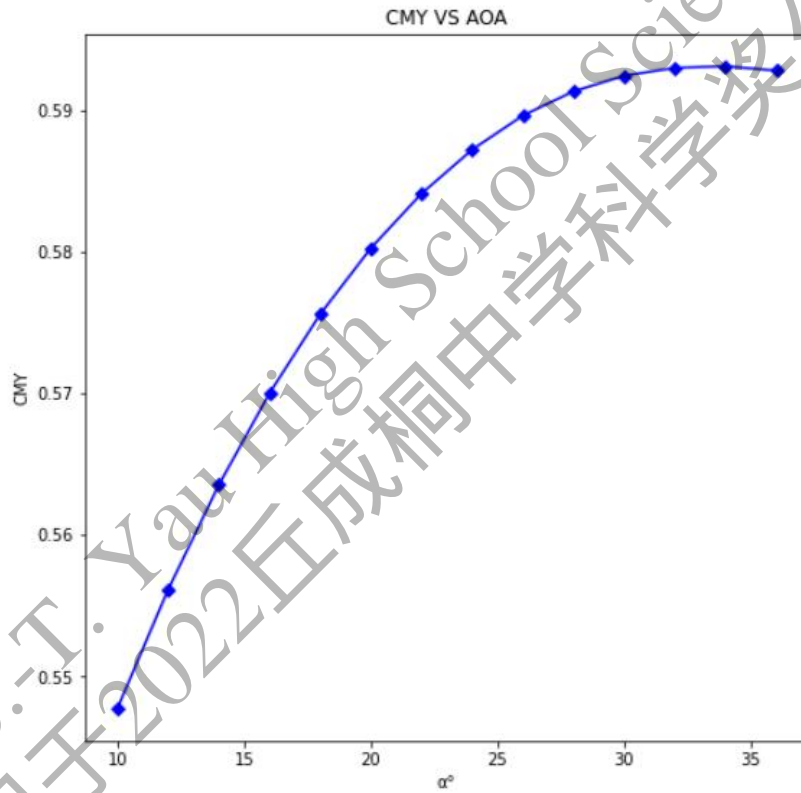

Fig3.8: CMY over angle of attack

As shown in Fig3.8, the stall angle can be obtained by the highest point of CMY/α curve, which is 34° for 20° deflection. The complete database for stall angle is shown:

23

Deflection angle/°	-20	-16	-12	-8	-4	0	4	8	12	16	20
Stall angle/°	22	24	26	22	18	14	15	16	22	30	34

Fig3.9: Table of deflection angle and corresponding stall angle

As shown in Fig3.9, downward deflection gives a maximum increase of 20° in stall angle at 20° deflection and upward deflection gives a maximum increase of 12° in stall angle at −12° deflection in comparison with the NACA-0012 finite wing.

4   Fabrication and Actual Flight

In this section, a morphing wing is built as designed in Section 2.2. The morphing wing is embedded on a RC model and a series of actual flight experiments is conducted and the aerodynamic database obtained by CFD simulation is verified. However, due to restrictions of flight by Civil Aviation Authority of Singapore(CAAS), flight test on cruise condition is not eligible. Hence, only flight tests on take off stage is conducted for various downward deflection angles.

4.1   Fabrication of The Morphing Wing and Test Model

In order to achieve a steady structure and light weight, balsa wood which is a conventional material of RC model is adopted to build the fixed section of a wing rib. Polyvinyl chloride is adopted to build the flexible trailing-edge by 3D printing for its flexibility. As shown in Fig4.1, a SG90 servo is embedded on the wing rib to control the trailing edge deflection.
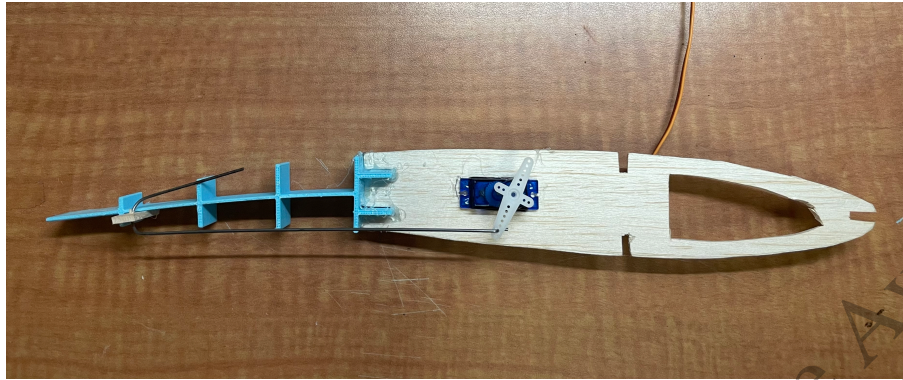
Fig4.1: A single morphing section

Each servo is powered by Raspberry Pi independently as a morphing actuator to provide the corresponding torque for deflection configurations. Each half-wing contains one fixed wing rib at the root and four morphing sections along the span, the wing ribs are connected by balsa wood sticks and carbon fiber rods to provide support for the mechanical structure. The leading edge of the wing is covered by 0.5mm to preserve the airfoil feature and the whole wing is covered with heat shrinkable film as the skin. The RC model for flight experiment is shown:

Fig4.2: RC model to conduct actual flight experiments

4.2 Experimental Results

Actual flight experiments on take off stage are conducted. The plane slid on the runway with engine running on full power with all downward deflection angles. Take off time is defined as from the start of sliding stage to the instant where the back landing gear left the ground. Six flights were conducted and the take off times were measured and recorded by stop watch.
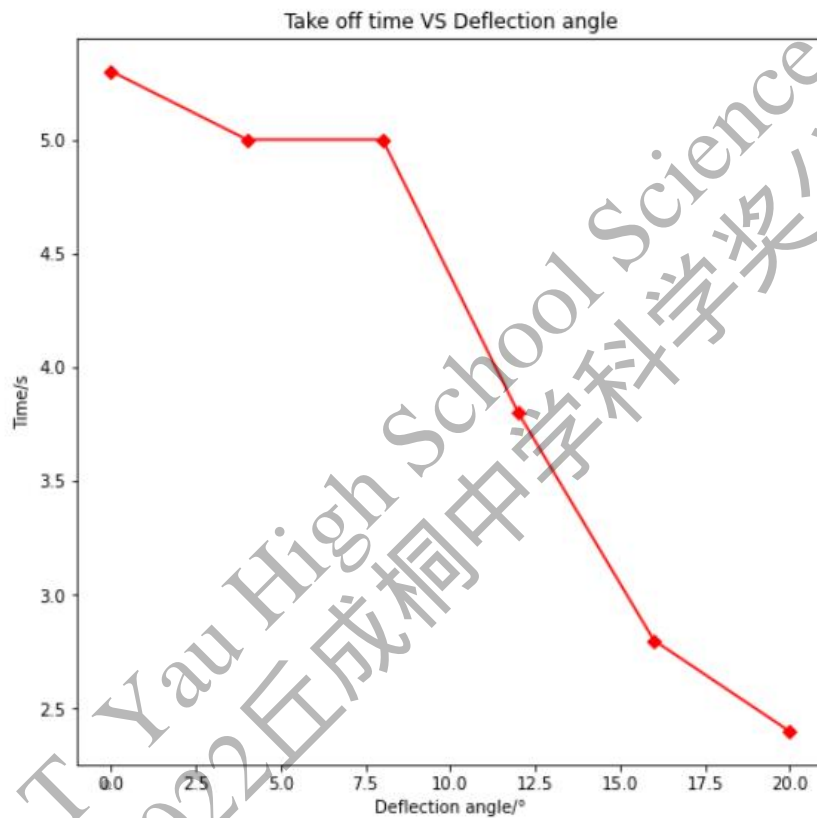

Fig4.2 Take off time of different morphing configurations

As shown in Fig4.2, significant decrease in take off time is observed starting from 12° deflection, the shortest take off time of 2.4s is achieved at 20° deflection. This verifies the CFD result in Fig3.5 that 20° downward deflection gives the highest coefficient of lift from 10° to 16° angle of attack.

26

5 Self-adaptive System

In this section, a self-adaptive system of morphing wing is introduced based on the database obtained by CFD simulation. The self-adaptive system contain two functions designed for take-off-landing stage and cruise stage respectively.

5.1 Take-off-landing Function

Downward deflection configurations are adopted for take off and landing stages in order to obtain higher coefficient of lift and achieve larger take off/landing angle of attack. The function of this stage is a one-to-one function and is defined as:

$$\mathbf{T}(\alpha_i) = \theta_i \tag{20}$$

where each angle of attack from 10° to 34° is related to a morphing angle respectively. In order to achieve higher coefficient of lift C_L and stall angle α, the flexible trailing-edge will deflect to 20° downward from 10° to 16° angle of attack, 16° downward from 18° to 30° and to 20° downward from 30° to 34°.
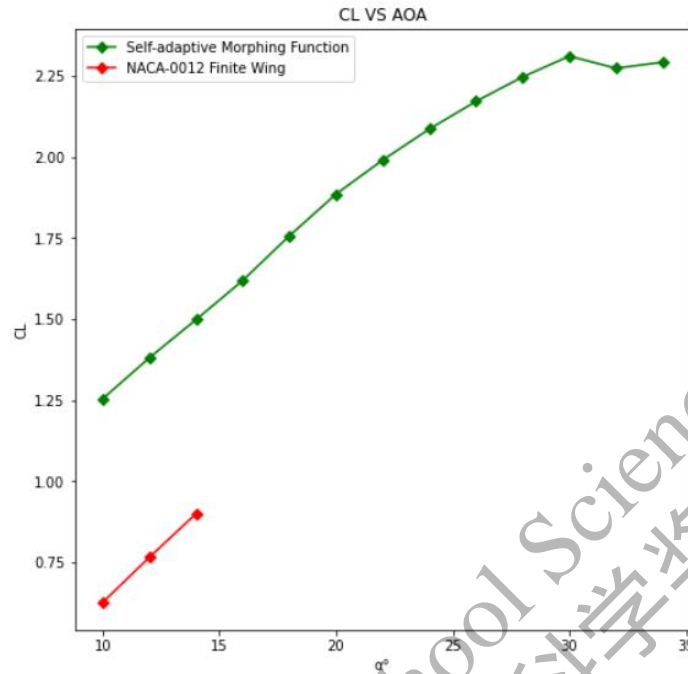
Fig5.1 Comparison of self-adaptive function and NACA-0012 finite wing

As shown in Fig5.1, the self-adaptive system gives a significant increase in coefficient of lift for all angles of attack and delays the stall angle from 14° to 34°. This allows the plane to have larger lift force and higher stall angle which allows the plane to have larger takeoff weight and shortened takeoff/landing distance. The flow field of selected flow conditions are presented to better illustrate the aerodynamic performance of self-adaptive system:
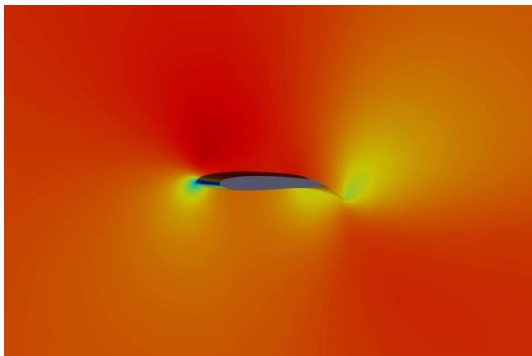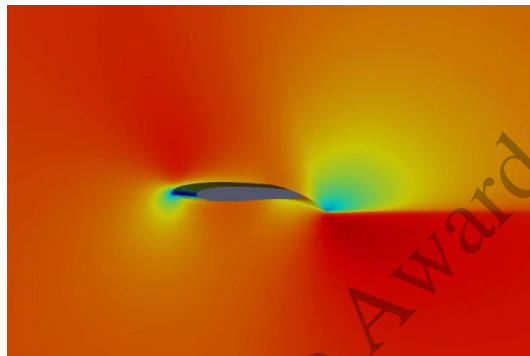
Figure 3: $\alpha = 10°$

Figure 4: $\alpha = 16°$

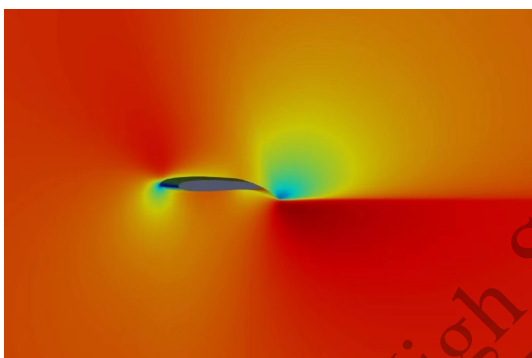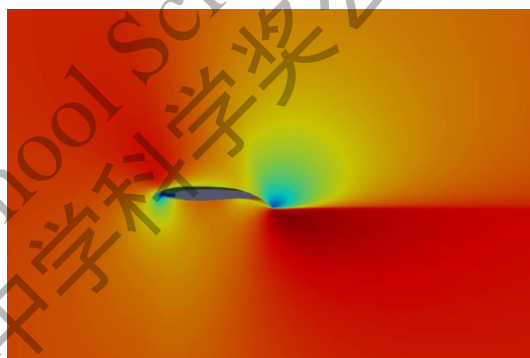Figure 5: $\alpha = 22°$

Figure 6: $\alpha = 26°$

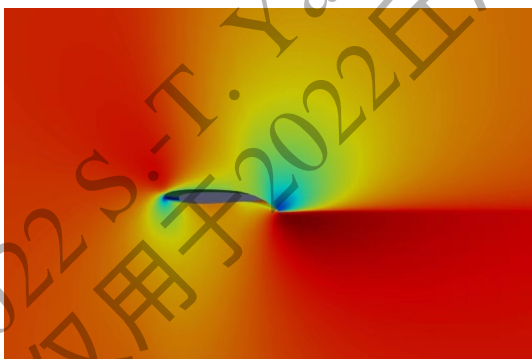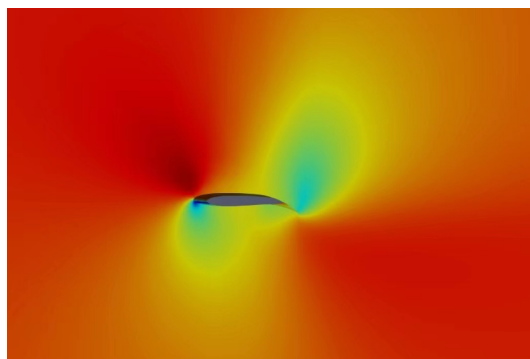
Figure 7: $\alpha = 30°$

Figure 8: $\alpha = 34°$

29

5.2 Cruise Stage Function

The cruise stage function can be applied in specific flow conditions for air crafts to maintain a constant lift coefficient under different angles of attack. This enables the air craft to maintain a constant height during cruise condition and hence conduct special missions such as docking, berthing, aerial refueling and so on. The function of this stage is defined as:

$$\mathbf{F}(C_{Li}) = \mathbf{S}_i \tag{21}$$

where each element $\mathbf{S}_i$ in $\mathbf{F}$ is corresponded to a C_L required and is a function of θ_i and α_i. The morphing wing is able to deflect according to the lift coefficient required to maintain the height of the plane at different angles of attack. The flow field of selected flow conditions are presented to better illustrate the aerodynamic performance of cruise stage function:
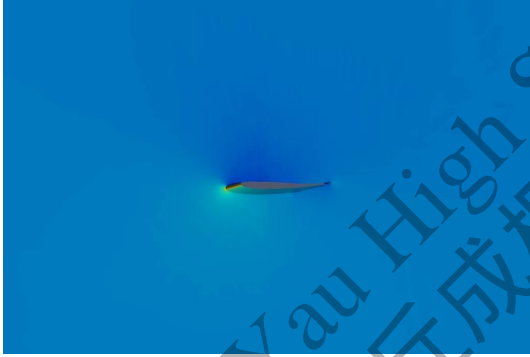

Figure 9: $\alpha = 16°$, $\theta = -8°$

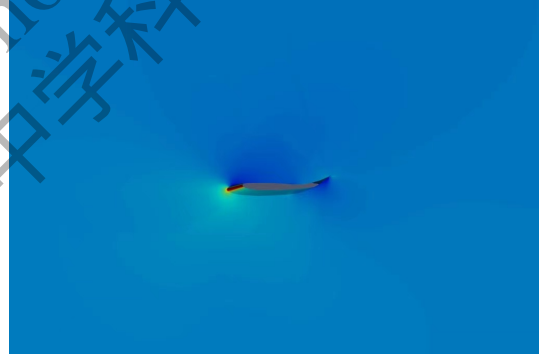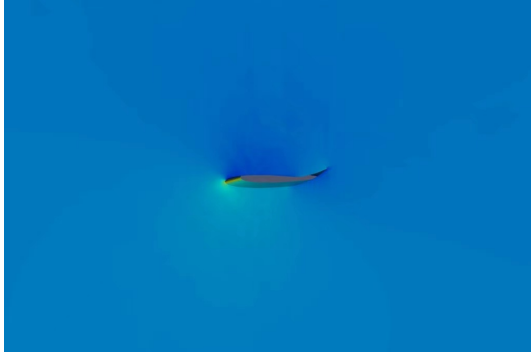Figure 10: $\alpha = 16°$, $\theta = -16°$

Figure 11: $\alpha = 16°$, $\theta = -20°$
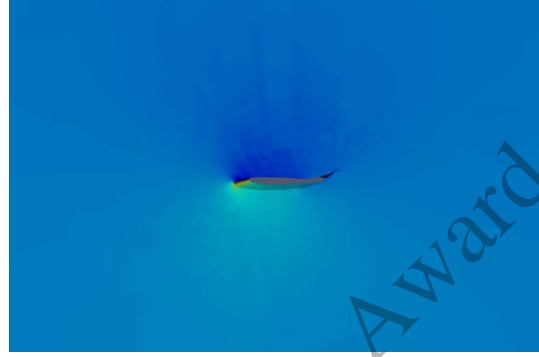

Figure 12: $\alpha = 30°$, $\theta = -20°$

As shown in figures, the upward deflection creates a high-pressure zone near the trailing-edge and hence shift the low-pressure zone towards the leading-edge. This maintains the lift coefficient when angle of attack increases.

6 Conclusion

6.1 Results Evaluation

In this paper, The equations of the deflection curves are derived and the 3D models of morphing wing configurations are built. The aerodynamic performances of different morphing angles and different angles of attack are studied and an efficient feedback control self-adaptive system is introduced. With the self-adaptive system, lift near tip is increased to delay stall, stall angle of NACA-0012 finite wing is increased significantly from 14° to 34° and coefficient of lift is increased about 2 times. This gives air crafts larger take off weight and higher take off/landing angles which shortens the take off/landing distance. This is especially meaningful for rural areas or emergency conditions where take off/landing condition is tough. The cruise stage function also enables air crafts to maintain constant height at different angles of attack

31

during cruise condition and this allows them to conduct special missions.

6.2 Improvement

1) In order to balance between the accuracy and efficiency of CFD simulation, the Compressible Euler Equations is adopted as the solver of SU2. However, this is not able to simulate the situation where flow is detached from the wing. Hence, compressible Navier-Stokes Equations can be adopted for further simulation of flow separation to achieve more accurate stall prediction.

2) Wind tunnel experiment could be conducted for further verification of CFD database. Since wind tunnel experiment is able to carry out dynamic tests of different angles of attack and different morphing angles, the self-adaptive database can also be expanded.

References

[1] Li, D., Zhao, S., da Ronch, A., Xiang, J., Drofelnik, J., Li, Y., Zhang, L., Wu, Y., Kintscher, M., Monner, H. P., Rudenko, A., Guo, S., Yin, W., Kirn, J., Storm, S., & Breuker, R. D. (2018). A review of modelling and analysis of morphing wings. Progress in Aerospace Sciences, 100, 46–62. https://doi.org/10.1016/j.paerosci.2018.06.002

[2] Wikipedia contributors. (2022, July 6). Stall (fluid dynamics). Wikipedia. https://en.m.wikipedia.org/wiki/Stall_(fluid_dynamics)

[3] Yokozeki, T., Sugiura, A., & Hirano, Y. (2014). Development of Variable Camber Morphing Airfoil Using Corrugated Structure. Journal of Aircraft, 51(3), 1023–1029. https://doi.org/10.2514/1.c032573

[4] LI, D., GUO, S., HE, Y., & XIANG, J. (2012). NONLINEAR AEROELASTIC ANALYSIS OF A MORPHING FLAP. International Journal of Bifurcation and Chaos, 22(05), 1250099. https://doi.org/10.1142/s021812741250099x

[5] LU, W., TIAN, Y., & LIU, P. (2017). Aerodynamic optimization and mechanism design of flexible variable camber trailing-edge flap. Chinese Journal of Aeronautics, 30(3), 988–1003. https://doi.org/10.1016/j.cja.2017.03.003

[6] KAN, Z., LI, D., XIANG, J., & CHENG, C. (2020). Delaying stall of morphing wing by periodic trailing-edge deflection. Chinese Journal of Aeronautics, 33(2), 493–500. https://doi.org/10.1016/j.cja.2019.09.028

[7] Governing Equations in SU2. (2022, August 31). SU2. Retrieved August 31, 2022, from https://su2code.github.io/docs_v7/Theory/

[8] Anderson, J. D., Jr. (2022). Fundamentals of Aerodynamics (5th ed.). McGraw-Hill.